Irrigation Science
https://doi.org/10.1007/s00271-024-00985-9

ORIGINAL PAPER

Hydraulic performance analysis of new versus commercial nozzle design for pressurised porous media filters

Jonathan Graciano-Uribe[1] · Toni Pujol[1] · Miquel Duran-Ros[2] · Gerard Arbat[2] · Francisco Ramirez de Cartagena[2] · Jaume Puig-Bargués[2]

Received: 7 August 2024 / Accepted: 28 October 2024

Abstract

Rapid water filtration with pressurised porous media filters is extensively applied in drip irrigation systems. In double-chamber filters, the underdrains are fixed to the base of the inner plate to sustain the media above while draining water. Here, a new underdrain design intended to reduce the filter energy consumption is presented. The main difference with commercial underdrain units corresponds to the distribution of the slots, being in a horizontal plate to uniformise the flow trajectories inside the porous media. Both commercial and new underdrain designs have been tested in laboratory in both filtration and backwashing modes with three media types, two media heights, and superficial velocities ranging from 20 to 120 m h^{-1}. In filtration mode, results indicate that the new design reduces the filter pressure drop by 31% at 60 m h^{-1} in comparison with the commercial one. The exploration with an analytical model that correctly reproduces the filter pressure drop, reveals that its value at 60 m h^{-1} is only 15% higher than the ideal scenario (uniform flow throughout the porous media bed). In backwashing mode, the pressure drop in comparison with the commercial design is reduced by 65% at 80 m h^{-1}, while having the same trend for the bed expansion, which is also predicted by a simple analytical expression. Thus, the new underdrain design produces a more homogeneous fluidised regime than the commercial one at low-moderate superficial velocities.

List of symbols

A	Cross-sectional area of the filter (m^2)
CN	Commercial nozzle
C_2	Inertial resistance coefficient (m^{-1})
D,d	Diameter (m)
d_{eq}	Particle equivalent diameter (mm)
D_f	Filter diameter (mm)
D_i	Equivalent diameter for non-uniform regions i = 1, 2 (mm)
E	Expansion of the porous bed (%)
g	Acceleration of gravity (m s^{-2})
h	Height of the expanded bed (mm)
h_0	Height of the packed bed (mm)
k	Minor loss coefficient (-)
L	Duct length (m)
L_{eb}	Effective length of the packed bed (m)
L_{nu1}	Length of the packed bed with non-uniform flow (region 1) (mm), (m)
L_{nu2}	Length of the packed bed with non-uniform flow (region 2) (mm), (m)
L_u	Length of the packed bed with uniform flow (mm), (m)
MS	Glass microspheres
NN	New nozzle
P_h	Hydraulic power (W)
p_s	Pressure in the porous media (Pa)
Q	Volumetric flow rate (m^3 h^{-1})
Re	Reynolds number (-)
r_i	D_f/D_i ratio for i = 1,2 (-)
SS1	Silica sand 1
SS2	Silica sand 2
v	Mean flow velocity (m s^{-1})
v_{mf}	Minimum fluidisation velocity (m h^{-1})
v_s	Superficial velocity (m h^{-1})
α	Inverse of the permeability coefficient (m^2)
Δp	Pressure drop (Pa), (kPa)
Δp_f	Filter pressure drop (Pa), (kPa)

✉ Jonathan Graciano-Uribe
jonathan.graciano@udg.edu

✉ Toni Pujol
toni.pujol@udg.edu

[1] Department of Mechanical Engineering and Industrial Construction, University of Girona, C/Universitat de Girona 4, 17003 Girona, Catalonia, Spain

[2] Department of Chemical and Agricultural Engineering and Technology, University of Girona, c/Maria Aurèlia Capmany 61, 17003 Girona, Catalonia, Spain

Published online: 13 November 2024

Δp_s	Pressure drop in porous media (Pa)
Δp_w	Pressure drop in water only regions (Pa)
Δp_{wf}	Pressure drop in water only regions (friction term) (Pa)
Δp_{wl}	Pressure drop in water only regions (minor loss term) (Pa)
δ	Zeroth-order uncertainty δ_i: Instrument uncertainty
ε	Porosity of the expanded bed (-)
ε_0	Porosity of the packed bed (-)
λ	Friction coefficient (-)
μ	Fluid dynamic viscosity (Pa s)
ρ	Fluid density (kg m^{-3})
ρ_p	Particle density (kg m^{-3})
σ	Standard deviation
ϕ	Particle sphericity coefficient (-)

Introduction

Pressurised filtration by porous media is a common water treatment in many sectors, including microirrigation (Lamm et al. 2007) where a minimum operating pressure as well as a minimum water quality is required for the proper functioning of drip emitters (Anyango et al. 2024). Commercial filters for this application may vary in size, commonly ranging from 300 to 1500 mm inner diameter, with media capacities ranging from 50 to more than 1500 kg of media, often mono component with grain size equivalent diameter ranging from approximately 0.50–1.50 mm.

The particle deposition in the porous media bed during the filtration process reduces the interstitial volume, thereby increasing the differential pressure measured between the filter's inlet and outlet. The quantity of particles retained with respect to the inflow value determines the retention efficiency, which becomes one of the most relevant indicators of the media bed performance (Mesquita et al. 2019a). Experimental studies of the retention efficiency are laborious tasks that must be carefully carried out to provide reliable information. Those with pressurised porous media filters focused on drip irrigation applications have provided very important insights into the filtration process. Hunce et al. (2019) conducted a series of tests with different media to evaluate the filterability index proposed by Ives (1970), concluding that angular media presented a more effective index than round grains. This finding has also been experimentally confirmed by Song et al. (2024) in the study of porous media types for micro-irrigation filters. Duran-Ros et al. (2023) developed a direct technique to determine the amount of particles retained in different media sheets, which exposed the relevance of the top layers in the retention process at all flow rates. Related to the system dynamics, Mesquita et al. (2019a) observed the formation of preferential paths in the porous media for flow rates < 36 m h^{-1}, as well as of uneven top surfaces of the media bed for flow rates > 61 m h^{-1}, both effects implying low particle removal efficiency.

In addition to analyses with contaminants in water, the value of the filter pressure drop measured in tap water also emerges as an important parameter since it indicates the starting condition of the filtration cycle. Indeed, a low value of this pressure drop prolongs the filtration cycle as it ends when a preset threshold pressure difference is reached (Song et al. 2024). From the operational point of view, longer filtration cycles are preferred since fewer backwashing cycles are required, leading to savings in both energy and water consumption (Pujol et al. 2024). Experimental measurements with tap water are much simpler than with contaminated water, favouring the analysis of the hydraulic behaviour of pressurised filters with different media and accessories, such as diffuser (Mesquita et al. 2019b; Alcon et al. 2023) and underdrains (Bové et al. 2015; Pujol et al. 2016; Solé-Torres et al. 2019). Mesquita et al. (2012) experimentally tested three different commercial filters with three different media pointing out that accessories contributed significantly to the filter pressure drop. Later, Mesquita et al. (2019b), based on simulation data, designed a new diffuser type that increased the flow uniformity inside the filter tank above the top surface of the media bed. Recently, this design was built and tested in laboratory with promising results (Alcon et al. 2023), as it increased the flow homogeneity. The effect of the underdrain type on the filter pressure drop was pointed out by researchers such as Burt (2010) who carried out experiments with commercial pressurised porous media filters that used different underdrain technologies. In double-chamber tanks, several nozzles are distributed at the base plate of the upper chamber, retaining the media bed and releasing filtered water to the bottom chamber (Mesquita et al. 2012). The implications of simple incremental modifications of a commercial nozzle in a laboratory filter remarked the relevance of having a large open area to reduce the total pressure drop (Pujol et al. 2016). Besides nozzles, underdrain designs also include spike and wand type ones when single-chamber filters are used. The consequences of using different underdrain technologies (nozzle, spikes, and wands) were numerically investigated by Pujol et al. (2020b), who not only emphasised the relevance of the underdrain open area in the total filter pressure drop but also remarked the importance of their distribution to uniformise the flow and balance their working points.

In contrast to the filtration mode, in backwashing, water flows upwards to fluidise the bed, to detach the particles previously retained in the packed media, and to carry them out of the system. The backwashing mode lasts for a prefixed time, which varies depending on the application (see, e.g., Tao et al. 2023). The efficiency of the backwashing process is related to the capacity to recover the initial clean bed conditions (de Deus et al. 2016). The vigour of

the fluidisation regime depends on the upward superficial velocity value, with optimum conditions reached at ≈100% bed expansion increment with respect to the height of the packed bed since these conditions maximise the flow shear stress applied to the media grains (Amirtharajah 1971). Since 100% bed expansion is not attainable in practice in pressurised media filters, manufacturers recommend a backwashing flow rate ≈50% greater than the flow rate in filtration mode (see Graciano-Uribe et al. 2024). Under these conditions, the bed expansion reaches values on the order of 40–50%. In non-pressurised (gravity) media filters, experimental results of the fluidisation process have been used to validate new models that successfully predict the bed expansion (Kramer et al. 2020b), which have also been proven to be useful in pressurised filters (Graciano-Uribe et al. 2022). However, the application of succinct equations derived in gravity systems, such as the Richardson-Zaki model (Richardson and Zaki 1954), to assess the bed expansion in pressurised filters poses uncertainties as these types of models have been revisited adding more complexity in order to gain predictability (Kramer et al. 2019). Thus, experimental studies focused on the bed expansion process of commercial pressurised media filters for drip irrigation often rely on empirical fittings (de Deus et al. 2020), with a limited capacity for their generalisation to other designs. However, these studies have evinced the dependence of the bed expansion mainly on the porous media type and less on the filter design (de Deus et al. 2020). Although the height of the bed expansion is expected to depend essentially on the flow rate (thus being almost independent of the underdrain type), the pressure loss in backwashing becomes crucial to estimate the energy consumption (Graciano-Uribe et al. 2022).

Some of the authors cited above have contributed to share the knowledge concerning both the filtration and backwashing performance of commercial porous media filters. However, there still seems to be very few works regarding the real effects of modifying the inner filter accessories, as the underdrains, with the final purpose to reach ideal conditions in commercial filters (i.e., totally uniform flow within the packed bed). Such achievement would reduce the power consumption to the minimum permissible value, and would prolong the filtration cycles, providing relevant gains to the end user. This was the issue here tackled. Learning from these previous experiences suggested that a new nozzle design for a double-chamber pressurised media filter based on a horizontal plate with a large open area would greatly reduce the pressure drop in both working modes, thereby improving the functioning in filtration (energy savings and longer cycles), as well as in backwashing (energy savings). The objective of the present work was to validate the above hypothesis. Therefore, both commercial (benchmark) and new nozzle designs were tested in a laboratory pressurised media filter with three media types, two packed media heights, and different flow rates. Analyses were carried out for both filtration and backwashing modes. For completeness, the feasibility of adopting simple analytical expressions for predicting the pressure drop in filtration mode, and the bed expansion in backwashing mode, was also investigated.

The structure of the paper is as follows. In Materials and methods section the materials and methods required to carry out the experimental tests are defined. The laboratory results for both filtration (pressure drop) and backwashing (pressure drop and bed expansion) regimes are reported in Results section. The discussion of the results is found in Discussion section, where the contribution of different regions of the filter to the total pressure drop in filtration mode are determined, as well as the required hydraulic power in the two hydraulic regimes. The dynamics of the fluidised bed is also described in Discussion. Then, the assessment of the capabilities of two analytical models to reproduce the observed values of pressure drop and bed expansion is conducted. The discussion section ends by comparing the performance of the experimental filter with commercial data. Finally, the main conclusions are listed in Conclusions section.

Materials and methods

Experimental setup

The experimental layout consisted of a closed-circuit water system (Fig. 1) able to carry out experiments in both filtration and backwashing regimes with tap water. The main elements of the system, listed in sequential order from the water tank, were: centrifugal pump (PRISMA 20/4, ESPA, Banyoles, Spain), electromagnetic flowmeter (AFT25, G-FLOW, Galapagar, Spain, ± 1% accuracy), globe valve to adjust the flow rate, pressurised media filter, and screen filter (130 µm filtration mesh, Regaber, Parets del Vallès, Spain) to retain grains that sporadically might exit the media filter. The double-chamber pressurised media filter was a stainless-steel cylinder with an inner diameter $D_f = 200$ mm. The upper chamber of 607 mm height had a rectangular polymethyl methacrylate (PMMA) window to visualise the fluidisation process that was recorded with a video camera (HDR-CX105E, Sony, Tokyo, Japan). Pressure and temperature data were also recorded with digital manometers (LEO Record, KELLER, Winterthur, Switzerland, ± 0.07% accuracy) at filter's inlet and outlet, and at three vertical levels in the filter upper chamber separated 100 mm, the first being located 100 mm above the underdrain base plate (P3 in

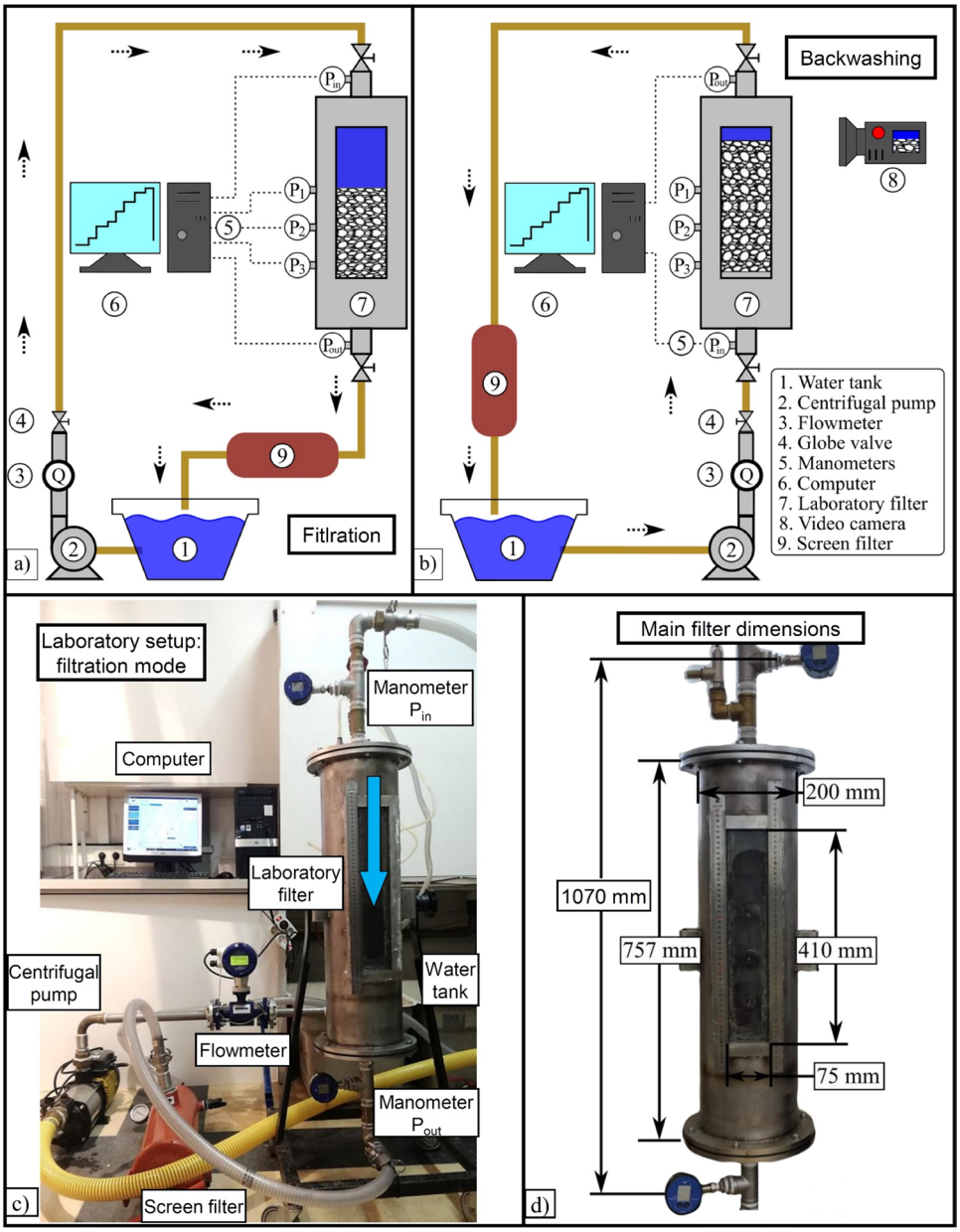

Fig. 1 Schema of the closed-circuit system in **a** filtration mode and **b** backwashing mode, **c** picture of the real setup in filtration mode, and **d** main filter dimensions

Fig. 1). The filter had a diffuser of circular shape of 120 mm diameter fixed 100 mm below the top cover.

Porous media

Three porous media types were tested. Silica sand (Sibelco Hispania, Bilbao, Spain) was dried and sieved to obtain two different grain size ranges (SS1 for 0.75–0.85 mm, and SS2 for 0.63–0.75 mm). Glass microspheres MS (Sovitec

Table 1 Physical characteristics of the porous media (Bové et al. 2015)

Property	Units	Silica sand 1 (SS1)	Silica sand 2 (SS2)	Glass microspheres (MS)
Grain size range	mm	0.75–0.85	0.63–0.75	0.63–0.75
Equivalent diameter (d_{eq})	mm	0.922 ± 0.019	0.715 ± 0.015	0.652 ± 0.014
Particle density (ρ_p)	kg m^{-3}	2510 ± 55	2410 ± 12	2437 ± 11
Packed bed porosity (ε_0)	–	0.40	0.42	0.38

Belgium, Fleurus, Belgium) were dried and sieved to the same grain size range as SS2 (0.63–0.75 mm). Physical properties of these media are listed in Table 1, where particle density ρ_p, porosity of the packed bed ε_0, and equivalent diameter d_{eq} defined as the diameter of a sphere with equal volume than the average volume of media followed Bové et al. (2015). However, the sphericity value ϕ, defined as the ratio between the surface area of the sphere with equivalent diameter d_{eq} and the actual surface area, is not reported in Table 1. This property is usually obtained from an indirect method that relies on the validity of the Ergun equation (e.g., Bové et al. 2015), which appears questionable in studies when the very same equation is adopted to propose an analytical model, as done in discussion. Therefore, the analytical models discussed in discussion were only applied to MS media since a sphericity value of $\phi = 1$ was accepted as a reasonable approximation from the microscopic observation of the shape of this media.

Nozzle types

Two nozzle designs were studied. The commercial nozzle was a classical pod-type design with 45 inclined rectangular slots of 30 mm × 0.4 mm cut in the frustoconical surface (Fig. 2). The total open area was 540 mm^2 which contrasted with the large cross-sectional area of the filter (= 31,416 mm^2). Besides, the discharge from the nozzle interior into the filter bottom chamber was made through a conduit of 16 mm diameter with an external thread to fix it to the lower side of the base plate. The design of the new nozzle intended to increase the open area in contact with the media, with 48 rectangular slots of 30 mm × 0.5 mm, and 40 rectangular slots of 15 mm × 0.5 mm, with a total open area of 1,020 mm^2 (89% more open area than the commercial design, see Fig. 2). The slots were cut in a stainless-steel horizontal plate (180 mm diameter) that almost occupied the entire cross-sectional area of the filter aiming to lessen the flow distortions within the media. The flow passage section to the filter bottom chamber was also enlarged in comparison with the commercial unit, using a 52.7 mm internal diameter pipe. A circular diffuser of 90 mm diameter inside the nozzle was bolted 28 mm above the bottom stainless-steel plate with the purpose to diminish the flow momentum, mainly for the backwashing regime (see Fig. 2).

Experimental procedure

Two packed bed heights $h_0 = 200$ and 300 mm were tested for each one of the three porous media types. Thus, 24 combinations (2 regimes, 2 nozzles, 3 porous media, and 2 packed bed heights) of the experimental set up were analysed at different superficial velocities ranging from approximately 20 m h^{-1} up to 120 m h^{-1}. This range included the average recommended values for filtration (57 m h^{-1}) and for backwashing (84 m h^{-1}, being 48% greater than that for filtration) of commercial pressurised porous media filters for drip irrigation (Graciano-Uribe et al. 2024).

The initial preparatory task for each test consisted in removing fines from the media by backwashing it inside the filter up to reach a water turbidity value at the outlet of the screen filter below 1.5 formazin nephelometric units (FNU). This process was repeated but in filtration configuration to guarantee the cleanliness of the water circuit. Then, with water in the system but flow at rest, the manometers were set to zero to get rid of the hydrostatic head, and set to record synchronously. In the experiments under backwashing regime conditions, the video camera was turned on, being vertically moved to follow the evolution of the top surface of the fluidised bed. Initially, the flow rate was adjusted to ≈ 0.6 m^3 h^{-1}, being increased up to the maximum value available by the pump (≈ 3.8 m^3 h^{-1}) at a rate of 0.3 m^3 h^{-1} in 11 intervals. For each flow rate, the last 30 s of data were gathered at 1 s interval to calculate both the average and the standard deviation of pressure data and, also in backwashing regimes, of the

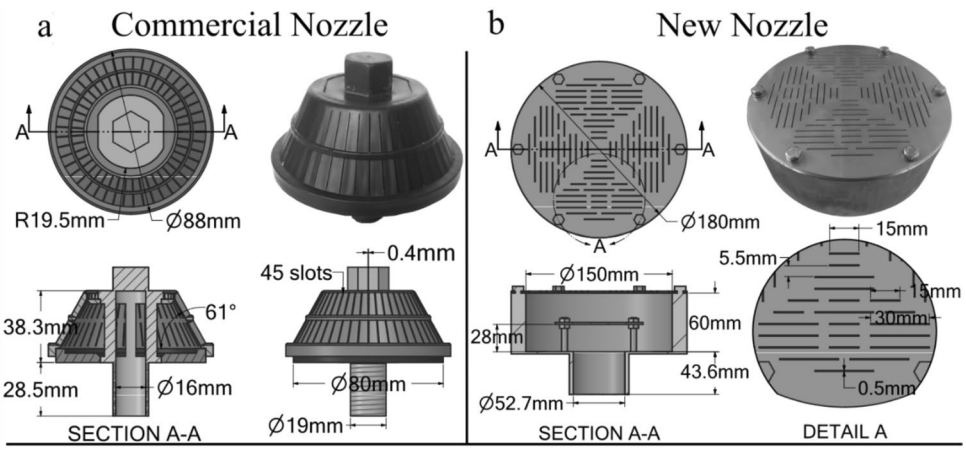

Fig. 2 Nozzles analyzed: **a** commercial nozzle, **b** new nozzle

expanded bed (identified as the highest level recorded). Note that in backwashing, some of the experiments for very large flow rates with the highest packed bed were not reported since the expansion reached levels above the top of the PMMA window. The previous procedure was repeated three times for all testing configurations.

The zeroth-order uncertainty of the measurement δ was calculated with the equation (Moffat 1988):

$$\delta = \sqrt{\delta_i^2 + (2\sigma)^2} \quad (1)$$

where δ_i is the uncertainty of the instrument, here taken equal to its accuracy value, and σ is the standard deviation of the set of 30 individual measurements acquired at 1 s interval for each experimental configuration. The error bars of the figures shown in results and discussion are obtained from applying the error propagation formulas (Moffat 1988) based on the zeroth-order uncertainty values δ.

Results

Filtration mode

Laboratory data confirmed the well-known dependence of the pressure drop with the media granulometry. At equal superficial velocity values and nozzle design, the flow through the packed media with the largest grains (SS1) produced the lowest total pressure drop (see Fig. 3 for $h_0 = 200$ mm and Fig. 4 for $h_0 = 300$ mm). The effect of increasing the nozzle open area in the new design had a clear impact on the reduction of the pressure drop in comparison with the frustoconical nozzle, especially when the flow

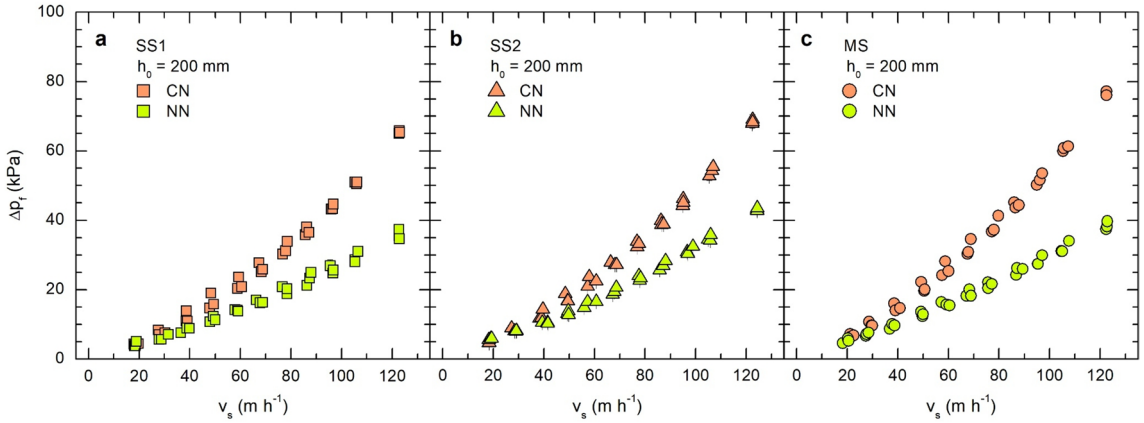

Fig. 3 Filter pressure drop for both commercial (CN) and new nozzle (NN) designs, as a function of the superficial velocity for different porous media: **a** SS1, **b** SS2, **c** MS. Height of the packed bed $h_0 =$ 200 mm. Error bars calculated from the zeroth-order uncertainty (Eq. (1)) are not visible since are smaller than symbol sizes

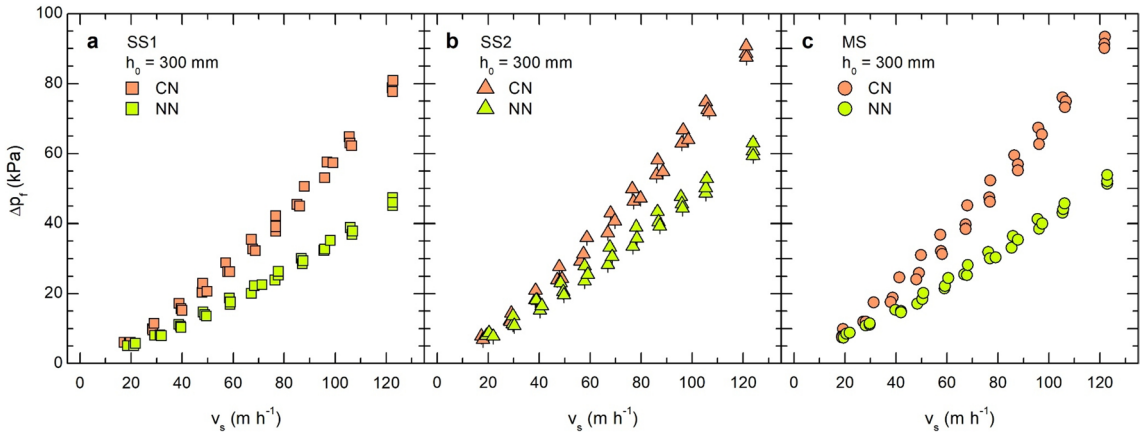

Fig. 4 Filter pressure drop for both commercial (CN) and new nozzle (NN) designs, as a function of the superficial velocity for different porous media: **a** SS1, **b** SS2, **c** MS. Height of the packed bed $h_0 =$ 300 mm. Error bars calculated from the zeroth-order uncertainty (Eq. (1)) are not visible since are smaller than symbol sizes

rate increased. At $v_s \approx 60$ m h^{-1} (approximately the average recommended value for commercial filters; Graciano-Uribe et al. 2024), the new nozzle was able to reduce the pressure drop with respect to the commercial design by 10.8, 8.6 and 6.5 kPa for MS, SS1 and SS2 media, respectively (mean values from Figs. 3 and 4). These figures corresponded to 36%, 34% and 23% reductions for MS, SS1 and SS2 media, respectively (mean reduction value of 31% when counting all media cases).

The pressure difference between data of Fig. 3 and of Fig. 4 was a consequence of adding 100 mm of media in the packed bed. Since the flow behaviour in this extra layer was not expected to be affected by the nozzle geometry at low-moderate superficial velocities, differences between Figs. 3 and 4 values were approximately the same for each nozzle, only being dependent on the media type.

Figure 5 was conceived to delve into the effect of the nozzle design on the pressure drop as it depicts only the pressure difference between a position 40 mm above the nozzle and the filter outlet. As noted by previous researchers (Mesquita et al. 2017), the nozzle design may strongly influence the flow within the porous bed near the slots, which have a remarkable contribution to the total pressure drop (Pujol et al. 2020b). Obviously, the nozzle design is also fundamental on how the flow is guided from the nozzle interior to the bottom chamber. In Fig. 5, data measured in manometer P3 (in Fig. 1) for the commercial nozzle was corrected to be properly compared with the new nozzle design. The latter element almost entirely occupied the cross-sectional area of the filter, being 60 mm high from the bottom inner plate (Fig. 2). Therefore, the manometer installed at position 3 in Fig. 1 had an effective height with respect to the new nozzle equal to 100–60 = 40 mm. Then, the vertical distance from manometer P3 and the horizontal plane 40 mm above the middle height of the commercial nozzle was 100.00 – (40.00 + 19.15) = 40.85 mm. Thus, for each scenario analysed, the pressure value assigned to the commercial nozzle in a location in the packed bed equivalent to that of the manometer P3 for the new nozzle design, corresponded to the readings of manometer P3 minus the pressure drop calculated for a packed bed of height 40.85 mm. The flow in this packed bed region was assumed to be uniform, with a pressure drop per unit length equal to that calculated from data of manometers P2 and P3 in Fig. 1. Note that at $v_s \approx 60$ m h^{-1}, pressure differences between the commercial and the new nozzle designs in Fig. 5 almost coincided with those previously mentioned for the total filter, being ≈ 9.4, 7.8, and 6.8 kPa for the MS, SS1, and SS2 media, respectively (averaged values for both initial packed bed heights from parabolic fits to data in Fig. 5). This result confirmed that, in terms of hydraulic pressure drop, the nozzle design influenced only the nearby region.

Backwashing mode

The behaviour of the bed expansion clearly depended on the porous media type (Fig. 6). Results for the media with the largest grain size (SS1) expanded the least as expected (de Deus et al. 2020), due to a higher downwards net vertical force (weight minus buoyancy) per grain. The bed expansion of both SS2 and MS media presented similar trends since grain sizes were within the same range, with the MS media consistently exhibiting higher fluidisation levels at equal flow rate values.

Although the experimental method was not devised to capture the minimum fluidisation velocity v_{mf}, the observations confirmed that the onset of fluidisation required higher superficial velocities for SS1 than for SS2, and for SS2 than

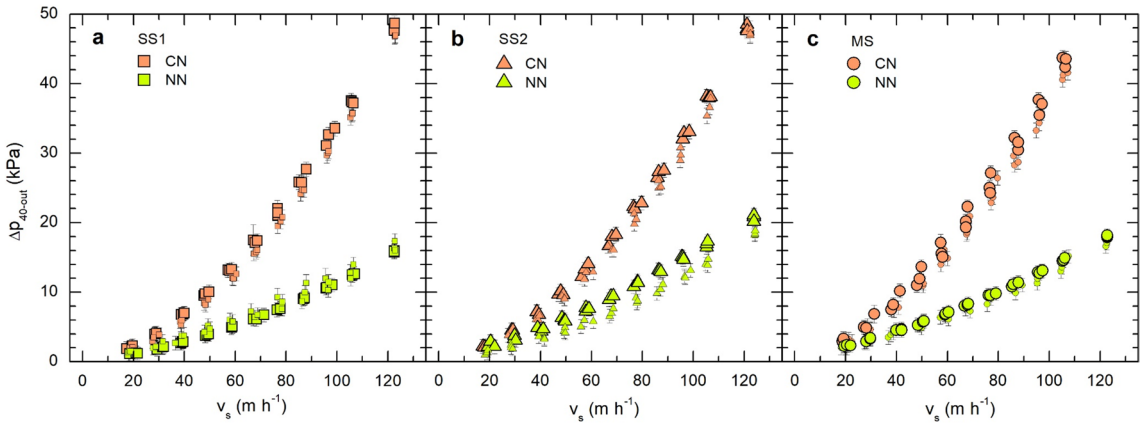

Fig. 5 Pressure drop between a location 40 mm above the new nozzle (NN) design or 40 mm above the mid height of the commercial nozzle (CN) design as a function of the superficial velocity for different porous media: **a** SS1, **b** SS2, **c** MS. Heights of the packed bed equal to h_0 = 200 mm for small symbols, and h_0 = 300 mm for large symbols. Error bars are calculated from the zeroth-order uncertainty (Eq. (1))

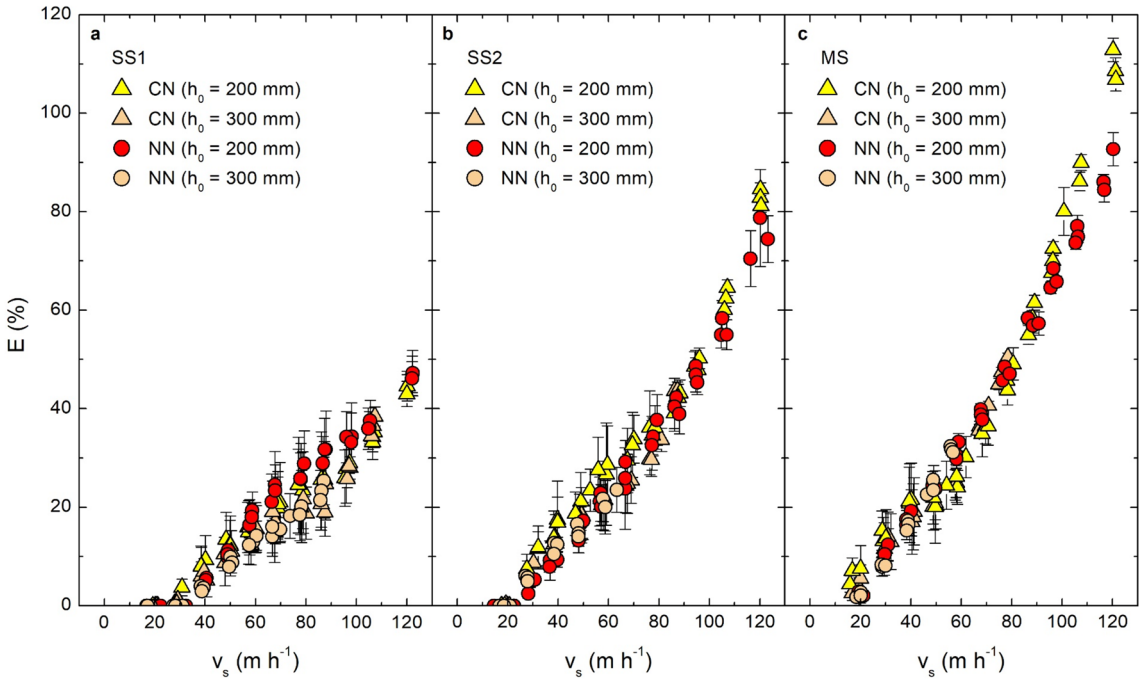

Fig. 6 Bed expansion as a function of the superficial velocity for different porous media **a** SS1, **b** SS2, **c** MS, using the new nozzle (NN) design, and the commercial nozzle (CN) design. Error bars are calculated from the zeroth-order uncertainty (Eq. (1))

for MS. Indeed, recordings displayed still beds up to ≈ 28 m h^{-1} for SS1, and up to ≈ 19 m h^{-1} for SS2, whereas the MS media already fluidised at the minimum velocity tested (≈ 16 m h^{-1}). These results are aligned with estimates of the minimum fluidisation velocity derived from an elementary analysis that equated the pressure force required to move the flow upwards through the media with the net downwards force (weight minus buoyancy) applied to the porous volume (Graciano-Uribe et al. 2022; v_{mf} = 23 m h^{-1} for SS1, v_{mf} = 16 m h^{-1} for SS2, and v_{mf} = 12.2 m h^{-1} for MS).

Related with the influence of the initial packed bed height, its effects on the bed expansion were more evident for the SS1 media with the new nozzle design, in which the case with h_0 = 300 mm reached lower heights of the fluidised bed at the same flow rate than with h_0 = 200 mm, especially at moderate superficial velocities (≈ 60 m h^{-1}). On the contrary, the expansion results were almost independent of the initial packed bed height when using the small granulometry and high uniformity of the MS media.

The bed expansion as a function of the superficial velocity experienced slightly different trends when changing the nozzle design. This variation was detected in the low and moderate (< 60 m h^{-1}) superficial velocity range, where the expansion in the commercial nozzle case raised monotonically with v_s up to a point where the growth seemed to stagnate (at ≈ 60 m h^{-1} in SS2 and MS media). In contrast, the bed expansion trend when using the new nozzle appeared to follow a more constant path, being similar to those experimentally observed with smaller devices that used horizontal screens covering all the cross-sectional area of the filter as underdrains (Graciano-Uribe et al. 2022). It is worth noting that the above-mentioned behaviour may be influenced by the filter's walls, whose effects are expected to be less pronounced in commercial filters with larger cross-sectional areas where multiple nozzles are present. From the above, it remains clear from Fig. 6 that, besides the porous media type, the dominant effect for determining the intensity of the bed expansion was the volumetric flow (or, equivalently, the superficial velocity) rather than the nozzle type.

At the recommended backflow values for commercial filters (≈ 80 m h^{-1}), the average bed expansion for all cases was 23.2% for SS1, 36.1% for SS2, and 49.1% for MS (data extracted from cubic fits), which corresponded to porosities of the expanded bed ε equal to 0.51, 0.57 and 0.58, respectively, being calculated from,

$$\varepsilon = \frac{\varepsilon_0 + E/100}{1 + E/100} \tag{2}$$

where $E/100$ is the dimensionless bed expansion value.

These bed expansion values were below the value (= 100%) expected to produce the maximum shear stress and, hence, with the maximum potential to hypothetically remove retained particles (Amirtharajah 1971). However, such elevated levels of fluidisation are impractical in

pressurised systems, but a minimum of 25% bed expansion value should be assured as this is the minimum commonly accepted for an effective particle removal (Brouckaert 2004). This value is reached for SS2 and MS media (averaged values for both nozzles with a cubic function fit to data) for v_s = 61.8 m h^{-1} and v_s = 52.8 m h^{-1}, respectively.

Regarding the filter pressure drop Δp_f during backwashing (Fig. 7), the behaviour per nozzle type became independent of the media type, and lightly dependent on the initial height of the packed bed. The commercial design presented a parabolic trend in terms of the superficial velocity, being very sensitive to the flow rate. In contrast, the results with the new nozzle described a much smoother increase in Δp_f. Obviously, the magnitude of the filter pressure drop in backwashing mode accounted for a fraction of that observed in filtration with tap water (Figs. 3–4) (e.g., 7.7 kPa for the commercial nozzle and 3.6 kPa for the new nozzle, both at ≈ 60 m h^{-1} for SS2 and h_0 = 300 mm, being 23% and 13% only of the values obtained in filtration with tap water, respectively). Nevertheless, the Δp_f registers in backwashing mode are of interest since they determine the energy consumption in that mode, and commercial filters may work at different regimes for both filtration ($v_s \approx$ 60 m h^{-1}) and backwashing ($v_s \approx$ 80 m h^{-1}) regimes. At the recommended backwash flow, the reduction of the filter pressure drop with the new nozzle design in comparison with the commercial one was 65% (the average value for all configurations was 11.1 kPa for the commercial design and 3.9 kPa for the new nozzle) (Fig. 7).

Discussion

Pressure drop contribution in filtration mode

Data from the manometers inserted in the filter body (P1, P2 and P3 in Fig. 1) were used to analyse the contribution of specific zones to the pressure drop. Since nozzles varied in size, raw data were corrected in order to represent the same type of information: pressure drop from the inlet to the top of the packed bed (inlet-media top; in-mt in Fig. 8), from the top of the packed bed to 40 mm above the slots (new nozzle) or to 40 mm above the vertical mid-point of the nozzle (commercial design) (mt-40 in Fig. 8), and from the latter point to the outlet (40-out in Fig. 8). The in-mt region was evaluated with the pressure difference between the manometers at inlet and at position P1 (Fig. 1), which was at or above the top of the packed bed in all cases except for the new nozzle with h_0 = 300 mm (the pressure drop in the region without media inside the filter body was assumed as very low). In the latter case, the top surface of the porous media bed was 60 mm above the manometer at P1. Therefore, the pressure drop equivalent to a 60 mm height of the packed bed was calculated from measurements at

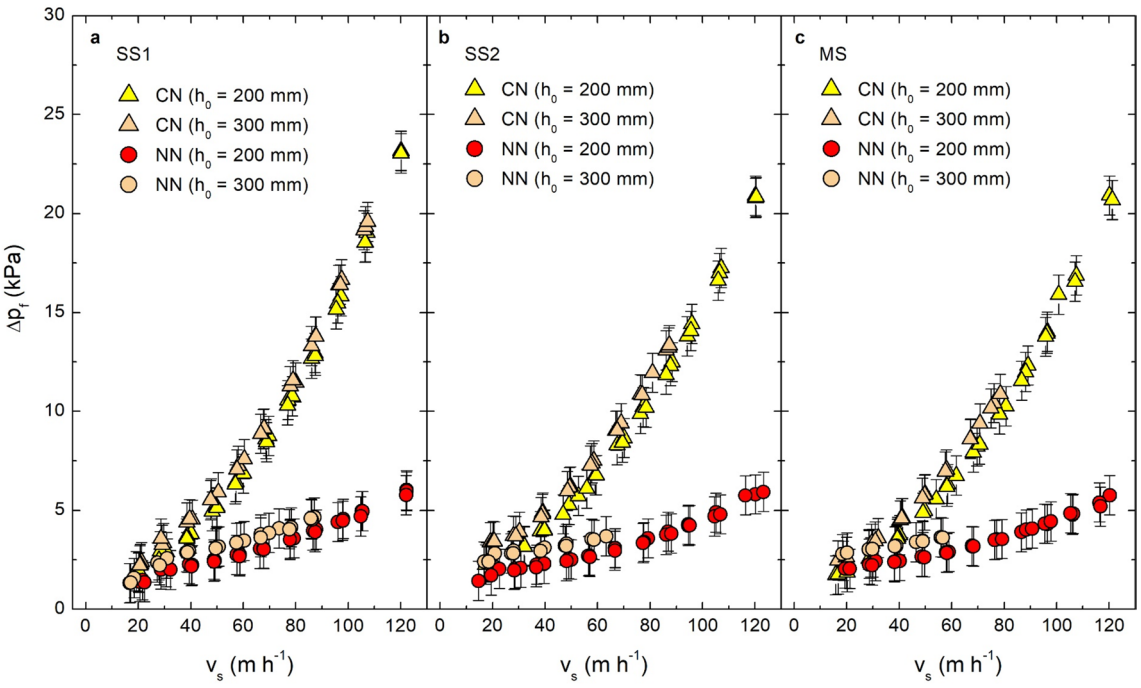

Fig. 7 Filter pressure drop in backwashing mode as a function of the superficial velocity for different porous media **a** SS1, **b** SS2, **c** MS, using the new nozzle (NN) design, and the commercial nozzle (CN) design. Error bars are calculated from the zeroth-order uncertainty (Eq. (1))

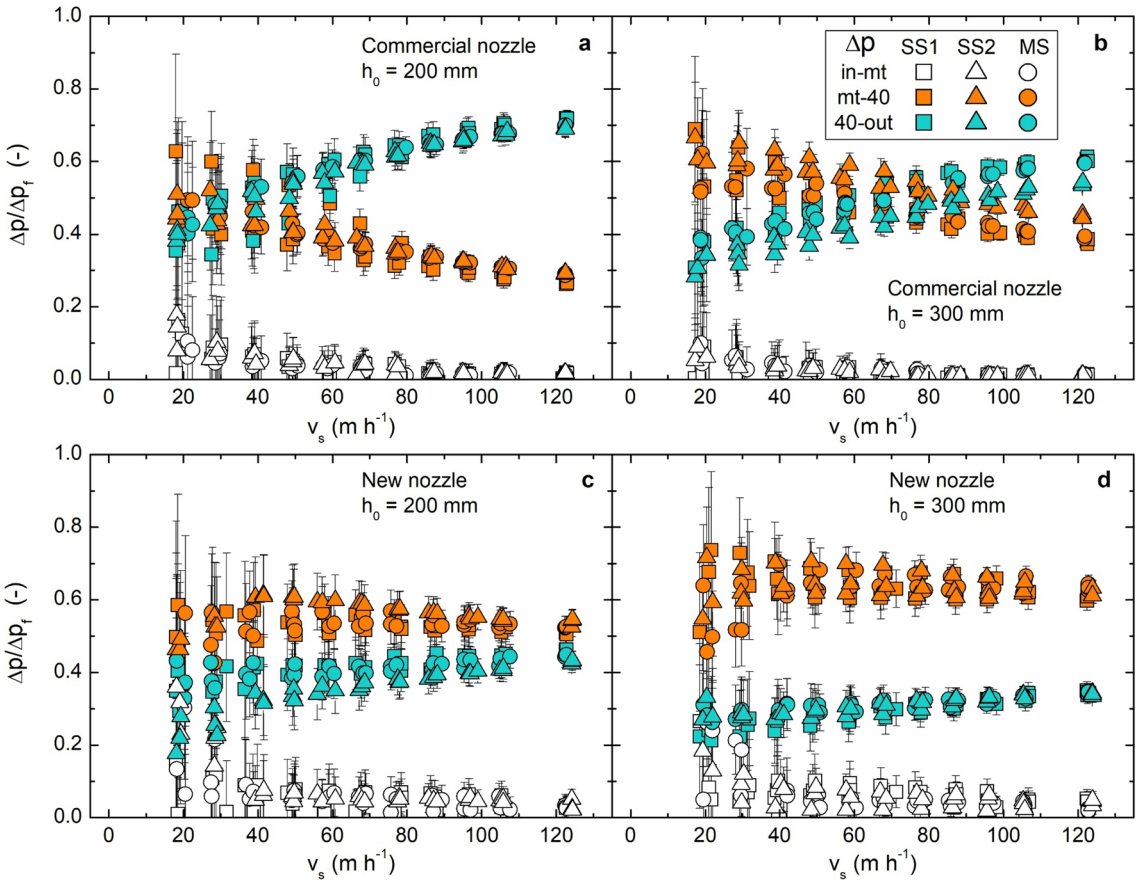

Fig. 8 Normalised pressure drop values for different regions: from filter inlet to the top surface of the porous media (in-mt), from the top surface of the porous media to 40 mm above the new nozzle or above the vertical mid-point of the commercial nozzle (mt-40), and from that point to the outlet (40-out) for the commercial nozzle and packed bed height **a** 200 mm, and **b** 300 mm; and for the new nozzle and packed bed height **c** 200 mm, and **d** 300 mm. SS1, SS2 and MS are the porous media types. Error bars are calculated from the zeroth-order uncertainty (Eq. (1))

positions P1 and P3 in Fig. 1, vertically separated 200 mm, and subtracted to the manometer at position P1 to estimate the in-mt pressure drop. The mt-40 pressure variation data was estimated from the pressure difference between the manometers at position P1 and at position P3 (Fig. 1). As discussed in results, the manometer at position P3 was not at 40 mm above the vertical midpoint of the commercial nozzle, so the pressure drop equivalent to a uniform flow within a packed bed of 40.85 mm height (calculated from manometers at positions P2 and P3) was added to manometer P3. The very same figure was subtracted from the pressure difference between manometers P3 and outlet to determine the 40-out pressure drop of the commercial nozzle.

In the commercial nozzle with a packed bed h_0 = 300 mm, the mt-40 and 40-out regions contributed similarly to the total pressure drop for superficial velocity values of 80 m h^{-1} approximately (Fig. 8b). This behaviour was also observed with numerical simulations of the laboratory filter (Graciano-Uribe et al. 2021). At the recommended values of superficial velocities for the filtration mode (≈ 60 m h^{-1}), the mt-40 and the 40-out regions contributed 56% and 41% to the Δp_f, respectively (SS2 case). In comparison, the new nozzle design (Fig. 8d) reached 65% and 29% for the same regions and SS2 case, clearly indicating the improving in the hydraulics of the underdrain.

The influence of the porous media type on the pressure drop per zones diluted at moderate-high superficial velocities, being only relevant at low superficial velocities. The contribution of the 40-out region to the total pressure drop increased as a function of the flow rate since the effect of the non-uniform flow region near the nozzle gained relevance. As a consequence of this prominent underdrain effect as the flow rate increased, the mt-40 contribution presented a continuous decline. Note that the pressure drop results per zones of the new nozzle design consistently offered trends with milder slopes than those of the commercial underdrain. Indeed, the ideal design would not experience flow concentrations in the porous media near the underdrain, so

the normalised contribution to the pressure drop per zones would be independent of the superficial velocity. The scenarios with the lowest packed bed (h_0 = 200 mm, Fig. 8a, c) displayed similar patterns than for the highest one (h_0 = 300 mm, Fig. 8b, d), although with increasing relevance for the 40-out region (or, conversely, less relevance for the mt-40 zone), as expected.

Hydraulic power

The hydraulic pumping power (P_h) of the system can be obtained from,

$$P_h = Q\Delta p_f \tag{3}$$

where Q is the volumetric flow rate, and Δp_f the filter pressure drop. Thus, the relative difference in the pumping power for both nozzle designs operating at the same flow rate (e.g., at the recommended superficial velocity) is nothing but the relative variation of the total filter pressure. Thus, Figs. 3 and 4 may be also used to determine the benefits of the new nozzle design in terms of savings in hydraulic power. In backwashing mode, the decision process to set the value of the superficial velocity depends on the extent of the bed expansion. Common practices consider values of 40–50% of the expanded bed for positive backwashes. In this case, the hydraulic power per unit of filter cross-sectional area greatly varied between nozzle designs (Fig. 9). For the SS2 media, the pumping power required for conditions of E = 50% for the new nozzle design was less than half the value needed for the commercial nozzle. Note that the trend for both nozzle designs at low bed expansions (i.e., low flow rates) were almost indistinguishable. Differences between designs were clearly observed for E > 10% (SS1) and E > 20% (SS2 and MS), beyond which the commercial nozzle design demanded more power for the same increment of the expanded bed than that required at the onset of the expansion conditions. Remarkably, the results for the new nozzle almost continued with the linear trend observed at the incipient stages of fluidisation, which implied a more efficient behaviour than the filter with the commercial nozzle (lower power consumption for the same expansion level). The efficiency of the new nozzle under backwashing conditions was patently obvious when comparing with data obtained from other experimental nozzles with both open and discharge areas to the bottom chamber similar to the commercial design, but with different shapes (Graciano-Uribe et al. 2024).

Fluidised bed dynamics

The video recordings of the fluidised bed dynamics indicated that the new nozzle design presented a more uniform fluidisation behaviour than the commercial nozzle for low

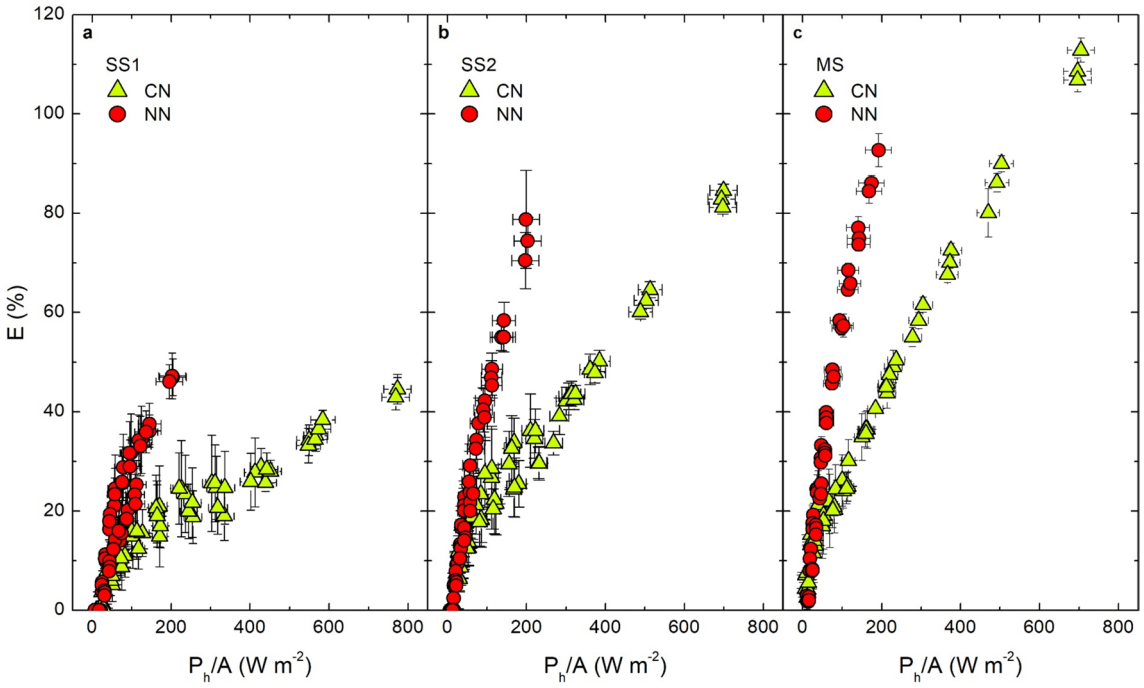

Fig. 9 Bed expansion as a function of the hydraulic power per unit of filter cross-sectional area for the commercial nozzle (CN) and the new nozzle (NN) with **a** SS1, **b** SS2, and **c** MS porous media types. Error bars are calculated from the zeroth-order uncertainty (Eq. (1)). Data for both initial packed bed heights are used

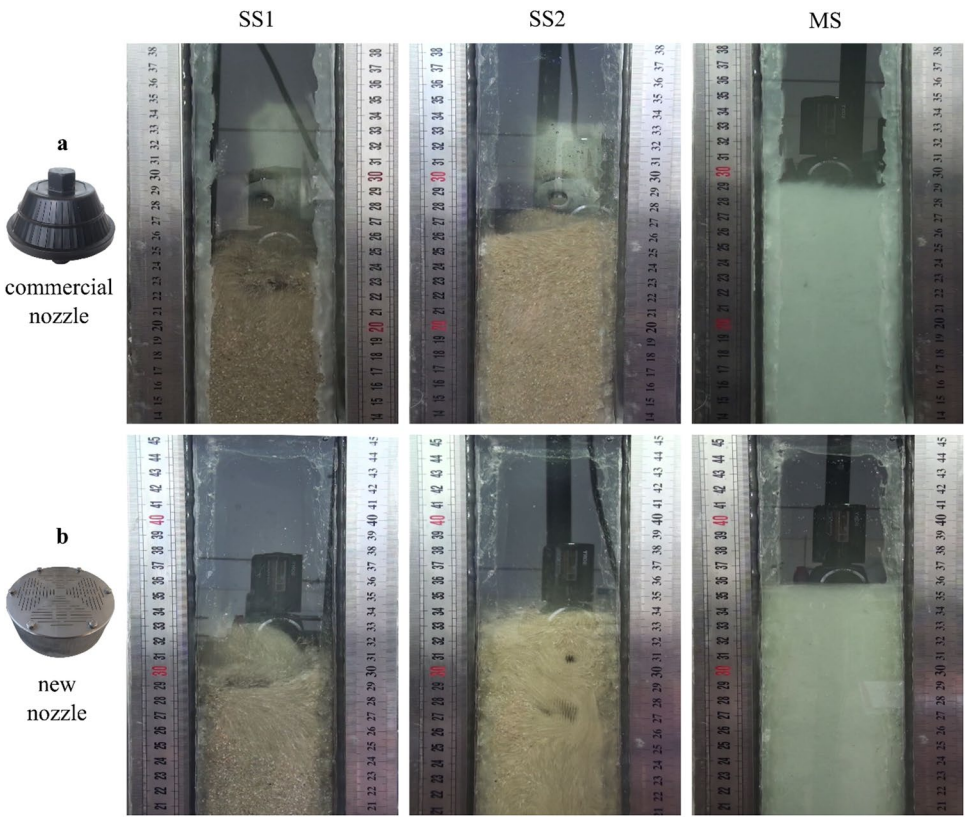

Fig. 10 Images of the expanded bed for **a** the commercial nozzle (CN) and **b** the new nozzle (NN) for all porous media types at $v_s \approx 77$ m h.$^{-1}$

and moderate superficial velocities (< 80 m h^{-1} in both MS and SS2 media). In this range of flow rates, the top surface of the expanded bed did not fluctuate as much as with the frustoconical design (Fig. 10), likely due to the distribution of the horizontal slots in the nozzle that almost occupied the entire cross-sectional area of the filter. Note that the Reynolds number *Re* in the filter tank for $v_s = 80$ m h^{-1} was $Re \approx 4440$, being almost equal to the corresponding value of the end of the transition zone to turbulence reported from the analysis of pressure data in pipes (White 2009). On the other hand, the commercial nozzle had inclined slots, whose outlet flow could be redirected by the filter walls, increasing the observed variability of the height of the expanded bed in comparison with the new nozzle design, particularly for the case with minimum packed bed height (h_0= 200 mm). At very large superficial velocities (> 100 m h^{-1}, $Re >$ 5560), intense fluctuations appeared with the new nozzle, experiencing a clearly turbulent bubbling phenomenon at the top of the fluidised bed (especially for the SS2 case), leading to important variations in the bed height measurements. This effect was slightly milder with the commercial nozzle, where the effect of the walls in this turbulent regime was not as important as before.

Analytical models

Several approaches have been developed to simulate the retention of particles by porous media (Zamani and Maini 2009). The macroscopic one relies on phenomenological models where the pressure gradient in the packed bed varies in terms of the mass of deposited particles (Herzig et al. 1970). As a result, the filter pressure drop increases with the filtration time. Although this process is out of the scope of the current analysis, the reduction of the pressure drop with tap water achieved by means of modifying the design of commercial elements has the potential to prolong the filtration cycle. Hence the importance of developing a simple model able to determine the pressure differential across the entire filter when using tap water. Here, the analytical model described in Graciano-Uribe et al. (2021) has been applied to both the new and the commercial nozzle cases. Essentially, the model assumes that the system can be interpreted as a series configuration of different elements that produce energy losses. By excluding the hydrostatic head from the calculations, and since both inlet and outlet pipes are of equal diameter, the pressure variation through the filter Δp_f can be expressed as the summation of friction and local head losses (multiplied by the specific gravity). The terms that contribute to Δp_f may be divided into,

$$\Delta p_f = \Delta p_w + \Delta p_s \tag{4}$$

where Δp_w refers to the pressure drop for those regions with only water, and Δp_s corresponds to the pressure drop within the porous media.

Pressure drop values for only water regions follow $\Delta p_w = \Delta p_{wf} + \Delta p_{wl}$ with Δp_{wf} the friction term, and Δp_{wl} the local term, being

$$\Delta p_{wf} = \lambda \frac{L}{D} \frac{\rho v^2}{2} \tag{5}$$

$$\Delta p_{wl} = k \frac{\rho v^2}{2} \tag{6}$$

where ρ is the water density, λ the friction coefficient, L the length of a duct with diameter D, and v the mean flow velocity. For the local term, k is the minor loss coefficient.

The elements contributing to the friction pressure drop, listed in sequential order from the inlet were: inlet pipe $\Delta p_{wf,i}$, filter top chamber above the packed bed $\Delta p_{wf,t}$, underdrain outlet conduit $\Delta p_{wf,u}$, filter bottom chamber $\Delta p_{wf,b}$, and outlet pipe $\Delta p_{wf,o}$. For each one of these terms, the calculation of the friction coefficient depended on the flow regime, laminar or turbulent, the latter following the Blasius equation for smooth pipes since the maximum Reynolds number was below 10^5 for any condition (White 2009). The mean flow velocity for each one of the previous elements was obtained from applying the mass conservation equation. For the commercial nozzle, the main contribution corresponded to $\Delta p_{wf,u}$ due to the small diameter of the nozzle discharge tube. Since this diameter was substantially larger in the new nozzle design, both inlet and outlet pipes were the most relevant terms there.

The elements contributing to the local pressure drop, also listed in sequential order from the inlet were: flow expansion from the inlet pipe to the filter tank $\Delta p_{wl,ei}$, flow contraction plus expansion as it encounters the diffuser $\Delta p_{wl,ced}$, flow expansion from the slots into the nozzle interior $\Delta p_{wl,es}$, flow contraction inside the nozzle when entering into the underdrain discharging tube $\Delta p_{wl,cu}$, flow expansion at the exit of the underdrain discharging tube into the bottom chamber $\Delta p_{wl,eu}$, and flow contraction from the bottom chamber into the outlet pipe $\Delta p_{wl,co}$. For all these terms, the flow velocity in Eq. (6) was the maximum calculated in the section change from the mass conservation equation. The minor loss coefficient k in Eq. (6) followed the classical contraction ($k = 0.42(1 - d^2/D^2)$) and expansion ($k = \left(1 - d^2/D^2\right)^2$) expressions that depended on the equivalent diameters ($d < D$) at both sides of the section change (White 2009).

The previous 11 terms for the evaluation of the pressure drop in the water only regions were straightforwardly deduced from the expected flow path in the system. Four of these 11 terms corresponded to the effect of the nozzle that, in sequence from the upstream flow, were the expansion through the slots $\Delta p_{wl,es}$, plus the contraction into the underdrain outlet tube $\Delta p_{wl,cu}$, plus the friction in the underdrain outlet tube $\Delta p_{wf,u}$, plus the expansion from the underdrain outlet tube $\Delta p_{wl,eu}$.

The contribution related to the pressure drop in the porous media was derived from the Darcy-Forchheimer equation (Yazdchi and Luding 2012),

$$-\nabla p_s = \frac{\mu}{\alpha}\vec{v} + C_2 \frac{\rho}{2} |\vec{v}| \vec{v} \tag{7}$$

where μ is the dynamic viscosity, α is the inverse of the permeability, and C_2 is the inertial resistance coefficient. Both $1/\alpha$ and C_2 are parameters that depend on the media (Yazdchi and Luding 2012).

The model divides the packed bed into three regions. The upper most region is not affected by the underdrain, and, therefore, develops a uniform flow that, from Eq. (7), produces the pressure drop $\Delta p_{s,u}$,

$$\Delta p_{s,u} = \left(\frac{\mu}{\alpha} v_s + C_2 \frac{\rho}{2} v_s^2\right) L_u \tag{8}$$

where v_s is the superficial velocity, equal to $4Q/(\pi D_f^2)$ with Q the volumetric flow rate, and D_f the cross-sectional filter diameter, and L_u is the height of the packed bed with uniform flow (i.e., the height of this upper most region).

The next two regions exhibit a non-uniform flow as it is expected from the concentration of the streamlines as the flow approaches the slots. Note that the nozzle open area is smaller than the cross-sectional area of the filter, leading to an acceleration of the flow within the porous media near the slots. This behaviour was observed in computational fluid dynamics simulations, whose pressure profile within the packed bed up to the nozzle entry was correctly reproduced by adopting linear variations of the available equivalent diameter in two regions with non-uniform flow (Graciano-Uribe et al. 2021).

The first one of these regions was assumed to have an equivalent length L_{nu1} in which the cross-sectional area available for the fluid flow varied from the filter diameter D_f to an equivalent diameter D_1. The pressure drop $\Delta p_{s,nu1}$ in this region was expressed as (Graciano-Uribe et al. 2021),

$$\Delta p_{s,nu1} = \left[\frac{\mu}{\alpha} v_s + C_2 \frac{\rho}{2} v_s^2 \frac{\left(r_1^2 + r_1 + 1\right)}{3}\right] r_1 L_{nu1} \tag{9}$$

where $r_1 = D_f/D_1$.

The second non-uniform flow region had an equivalent length L_{nu2}, in which the cross-sectional area available for the flow varied, now, from D_1 to an equivalent diameter D_2. For this region, the pressure drop $\Delta p_{s,nu2}$ followed the expression (Graciano-Uribe et al. 2021),

$$\Delta p_{s,nu2} = \left[\frac{\mu}{\alpha}v_s + C_2\frac{\rho}{2}v_s^2\frac{\left(r_1^2 + r_1 r_2 + r_2^2\right)}{3}\right] r_1 r_2 L_{nu2} \quad (10)$$

where $r_2 = D_f/D_2$.

The equivalent diameter D_1 was calculated as the value that provided a circular area equal to the nozzle surface area (including the slots), whereas the equivalent diameter D_2 corresponded to the value whose circular area equalled the nozzle open area (slots only). The total length of the non-uniform region $L_{nu1} + L_{nu2}$ was calculated as the orthogonal distance from the surface of the nozzle with engraved slots to its virtual extrusion whose surface is equal to the cross-sectional area of the filter. The length L_{nu2} was assumed to be equal to half the mean distance between the centre of two neighbour slots. For the commercial nozzle, D_1= 108.5 mm, D_2= 26.2 mm, L_{nu1} = 31.1 mm, L_{nu2} = 1.7 mm. For the new nozzle design, D_1= 144.0 mm, D_2= 36.0 mm, L_{nu1} = 7.6 mm, L_{nu2} = 3.0 mm. The height of the packed bed with uniform flow was calculated as $L_u = L_{eb} - \left(L_{nu1} + L_{nu2}\right)$, where L_{eb} was the effective height of the packed bed (vertical distance from the top of the packed bed up to the midpoint of the commercial nozzle height, or to the top of the new nozzle).

If r_1 and r_2 terms in Eqs. (9–10) are greater than 1, the pressure gradient in the non-uniform region exceeds that in the uniform one. The limit $r_1 = r_2 = 1$ corresponds to a flow without streamlines concentration, so the pressure gradient in Eqs. (9–10) transforms into that of the uniform flow case, Eq. (8). Thus, the recommended nozzle design, in terms of hydraulic gradient, would be that with the minimum values of L_{nu1} and L_{nu2} and with r_1 and r_2 as close to 1 as possible.

The $1/\alpha$ and C_2 parameters in Eqs. (8–10) are media dependent, being obtained either directly by means of experimental data (Pujol et al. 2020a), or indirectly by association with well-known analytical equations (Erdim et al. 2015). In the latter approach, the Ergun equation is commonly assumed as a valid expression for monodisperse media (Graciano-Uribe et al. 2021), from which

$$\frac{1}{\alpha} = 150\frac{\left(1-\varepsilon_0\right)^2}{\phi^2 d_p^2 \varepsilon_0^3} \quad (11)$$

$$C_2 = 3.5\frac{\left(1-\varepsilon_0\right)}{\phi d_p \varepsilon_0^3} \quad (12)$$

where ε_0 is the packed bed porosity, d_p is the grain size diameter usually adopted to be equal to the equivalent diameter d_{eq}, and ϕ is the grain sphericity. The latter property, as previously explained, is the most challenging to determine experimentally (see, e.g., Cruz-Matías et al. 2019). Therefore, the previous model was only applied to the microsphere media where the assumption of $\phi = 1$ was reasonable.

Finally, the analytical model of the total pressure drop in the filter consisted in the summation of Eqs. (8–10) for the porous media plus the 11 terms of the water only regions. The results when applied to the MS media conditions for both nozzle designs and two packed bed heights adequately reproduced the measured trends

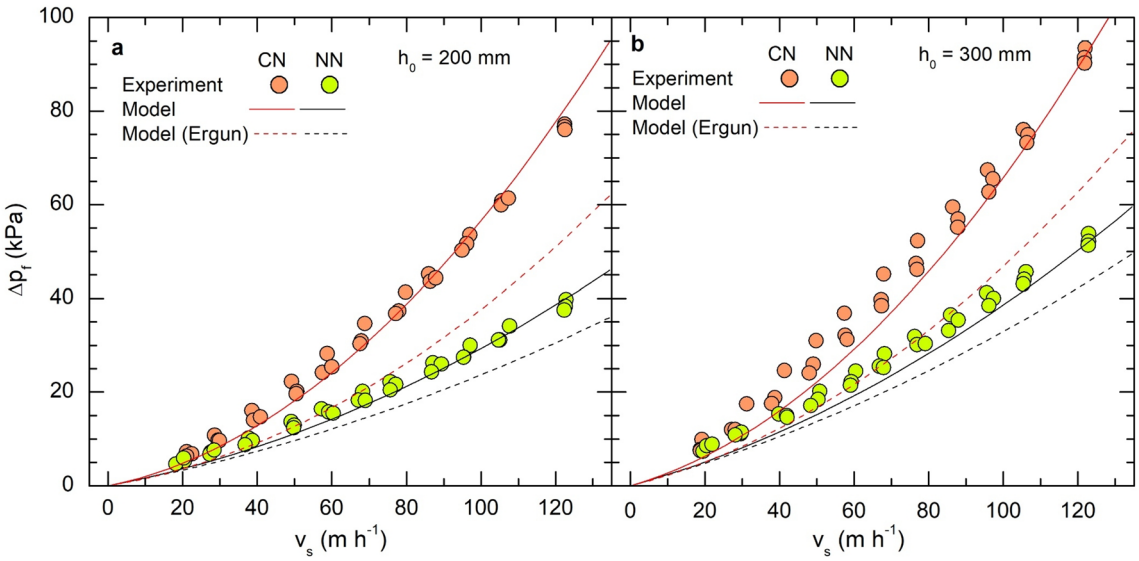

Fig. 11 Total filter pressure drop as a function of the superficial velocity with the commercial nozzle (CN) and the new nozzle (NN) designs for packed bed heights of microspheres a) 200 mm and b) 300 mm. Analytical model results for the CN (red line) and the NN (black line). Dashed lines correspond to the ideal case of uniform flow within the media bed. Error bars based on the zeroth-order uncertainty (Eq. (1)) are not visible since are smaller than symbol sizes

(Fig. 11). The main discrepancies with the measured pressure drop were obtained at $v_s \approx 60$ m h^{-1} for $h_0 =$ 300 mm where the analytical models for both new and commercial cases underestimated the data by 16.0%. For $h_0 = 200$ mm, the maximum difference occurred at $v_s \approx$ 46 m h^{-1} (commercial nozzle) and $v_s \approx 54$ m h^{-1} (new nozzle) where the model underpredicted the pressure drop values by 12.9% and 14.6%, respectively. The analytical model was based on the summation of major and minor losses expressed from the classical formulas used in piping systems (White 2009), ignoring dynamical interactions between the different elements of the filter, which might be the responsible of the observed discrepancies. Further analyses with data from other filter configurations would be required to fully determine the model capabilities.

For completeness, the results of the model with $L_u = L_{eb}$ and $L_{nu1} = L_{nu2} = 0$ (i.e., porous media with uniform flow only) are also displayed in Fig. 11 (dashed lines). In the latter, the solution clearly underpredicted the pressure drop of the entire filter, highlighting the relevance of the non-uniform flow regions within the packed bed to correctly interpret the system behaviour.

The solution for the Ergun case represented the ideal case with uniform flow throughout the entire packed bed. Therefore, the best nozzle design, in terms of reducing the pressure loss, would be that with a trend as close as possible to the dashed lines in Fig. 11. The new nozzle design, with its large open area, generated only 15% more pressure drop than the ideal conditions at $v_s = 60$ m h^{-1}, clearly improving the behaviour of the commercial nozzle whose increase was of 40% (obtained after averaging the data for the two initial packed bed heights).

From the hydraulic point of view, the nozzle could have also been interpreted as a single element with its corresponding minor loss coefficient. In this approach, the four pressure drop terms previously attributed to the underdrain ($\Delta p_{wl,es}$, $\Delta p_{wl,cu}$, $\Delta p_{wf,u}$, $\Delta p_{wl,eu}$) collapsed into one with the form of Eq. (6). The minor loss coefficient k was obtained by fitting the pressure drop data as a function of the superficial velocity extracted from the comprehensive nozzle model (four terms). The equivalent minor loss coefficient of the commercial nozzle was huge (k= 46,608), exceeding in more than 11 times the minor loss coefficient obtained for the new nozzle design (k= 3,964). For comparison purposes, these minor loss coefficient values were equivalent to those of a pressure reducing valve with an opening degree equal to 11.6% (commercial nozzle) or 24.0% (new nozzle) (Meniconi et al. 2016). A different approach to tackle the effect of the nozzle on the filter pressure drop was to consider it as a sudden contraction plus a sudden expansion (being a simplified version of the flow through an orifice). In this case, the effect of the nozzle would be equivalent to a reduction of the filter diameter from $D_f = 200$ mm to $d = 14.8$ mm (commercial nozzle) or $d = 27.3$ mm (new nozzle). These previous analyses clearly indicated the improvement of the hydraulic behaviour with the new nozzle.

On the other hand, the analytical approximation for the expansion of the fluidised bed was derived from the balance between the net downward force (weight minus buoyancy) applied on the porous media and the pressure force needed to push the flow upwards through it (Graciano-Uribe et al. 2022), which, per unit volume, is written as:

$$g\left(\rho_p - \rho\right)(1-\varepsilon) = 72\frac{\mu}{\phi^2 d_p^2}\frac{(1-\varepsilon)^2}{\varepsilon^3}v_s + 1.75\frac{\rho}{\phi d_p}\frac{(1-\varepsilon)}{\varepsilon^3}v_s^2 \tag{13}$$

where ρ_p is the media density.

In Eq. (13), the right-hand-side term corresponds to the pressure drop per unit length through the porous media based on the Darcy-Forchheimer (Eq. (7)), with the identification of Eq. (12) for the C_2 term, and of Eq. (11) for the $1/\alpha$ term multiplied by 72/150. The reason for the latter modification is based on the basic premise that, in contrast with the packed bed, an ad-hoc tortuosity term for the flow path (see McCabe et al. 1993) must not be added in the expanded bed analysis. Thus, the first term on the right-hand-side in Eq. (13) is interpreted as the pressure loss per unit length due to friction inside the porous media assuming a laminar flow, whereas the second one is interpreted as the minor pressure loss per unit length due to a series of flow contraction plus expansion as it encounters media grains inside the media (Graciano-Uribe et al. 2022).

For a fixed value of the superficial velocity (or, equivalently, flow rate), Eq. (13) has the form of a depressed cubic equation in terms of ε, with the existence of a single real solution. The porosity of the expanded bed is then used to calculate the expansion of the fluidised bed by applying the mass conservation equation, giving

$$\frac{h - h_0}{h_0} = \frac{\left(\varepsilon - \varepsilon_0\right)}{(1-\varepsilon)} \tag{14}$$

where h and h_0 are the heights of the expanded and packed beds, respectively.

As in the analytical model for the filter pressure drop in filtration mode, Eqs. (13–14) were applied for microspheres only since the sphericity value was set to $\phi = 1$. Despite the simplicity of the equation (more complex prediction models for determining the fluidised bed porosity are listed in Kramer et al. 2020a), the predicted bed expansion reasonable reproduced the observed trend (Fig. 12), except for low flow rates where the minimum fluidisation velocity conditions were not correctly captured, as expected from the modification of the tortuosity value.

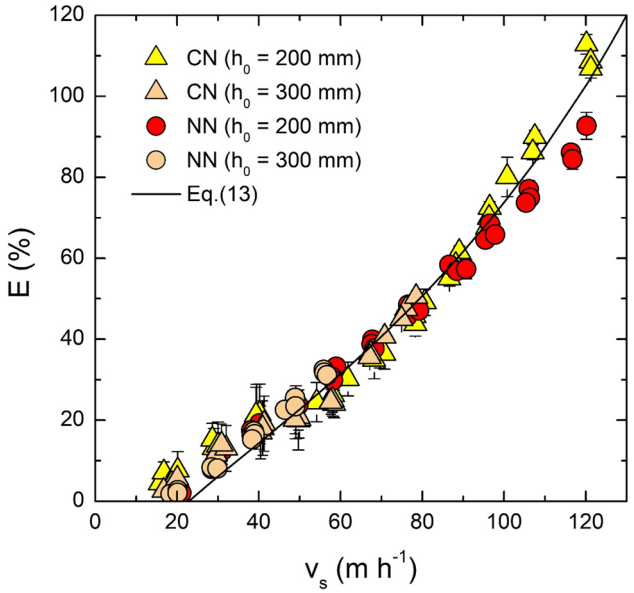

Fig. 12 Bed expansion as a function of the superficial velocity for MS media (as in Fig. 6c) but including the results from Eq. (13). Error bars are calculated from the zeroth-order uncertainty (Eq. (1))

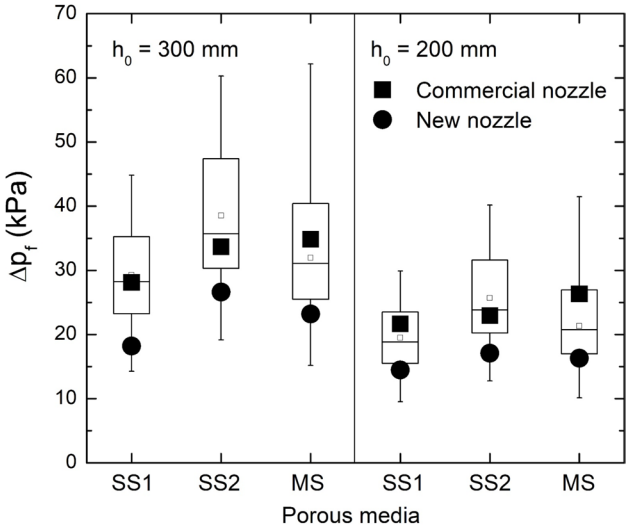

Fig. 13 Filter pressure drop at v_s = 60 m h^{-1} for different porous media types (SS1, SS2, MS) and packed bed heights (200 and 300 mm) for the commercial and the new nozzle design, and the equivalent box charts obtained from information of 33 commercial data. Hollow squares indicate the mean, and whiskers refer to 5% and 95% percentiles. Error bars of the experimental values (commercial and new nozzles) calculated from the zeroth-order uncertainty (Eq. (1)) are not visible since are smaller than symbol sizes

Comparison with commercial units

The degree of improvement of the new nozzle with respect to the commercial design was also examined by comparing the results with those obtained from state-of-the-art double-chamber media filters employed in irrigation. The screening of published data reduced the candidates to four manufacturers (30 models), and to the research of commercial units carried out by Mesquita et al. (2012) (1 model with three media type configurations), since provided the required information for the analysis (geometrical filter dimensions, pressure drop as a function of flow rate, media type, amount of media used, and/or packed bed height).

Raw data from datasheets were processed to provide the equivalent pressure drop for SS2, SS1 and MS media types with 200 and 300 mm packed bed heights at 60 m h^{-1}, which approximately represents the recommended superficial velocity for filtration (see, also, Graciano-Uribe et al. 2024). The normalisation procedure was based on assuming that the ratio $\Delta p_s/\Delta p_f$ was constant, and on accepting the relationship between variables offered by Eq. (7) and Eq. (11), with $C_2 = 0$ m^{-1} for simplicity, being equivalent to the dependence of variables of the well-known Carman-Kozeny equation (Holzer et al. 2023). Thus, for example, if the packed bed height calculated from manufacturer's datasheet was h, these data were normalised by a factor equal to h_0/h to represent h_0 conditions, since the Carman-Kozeny equation predicts a linear relationship of Δp_s with h_0.

Results revealed a marked variability (Fig. 13), not only for the wide range of filter dimensions encompassed (diameters from 200 to 1500 mm; see Supplementary Information), but also for the vague characterisation of the media type often reported in some datasheets. Despite these concerns, the pressure drop measured with the commercial nozzle was located close to the median for SS1 and SS2, with the new nozzle data clearly falling below the 25th percentile. These results demonstrated the potential of the new design in reducing the pressure drop. Although this conclusion could be dubious by observing the MS data, where the experimental results with the commercial nozzle approach the 75th percentile, the effect of the new design for MS triggered the most remarked decline in the pressure drop for all media at both packed bed heights.

Conclusions

A new nozzle design for pressurised porous media filters was designed and experimentally tested in filtration (tap water) and backwashing modes with three media, two packed bed heights, and different flow rates.

In filtration mode, the new nozzle reduced the total filter pressure drop of the commercial case by 26% and 21% at v_s = 60 m h^{-1} for a packed bed height equal to 200 mm, and 300 mm, respectively (SS2 media case). The filter pressure drop reduction obtained with the new nozzle increased with the grain size, media sphericity, and flow rate.

In backwashing mode, the trend of the expanded bed at large superficial velocities was very similar for both nozzle designs. However, the major open area of the new nozzle penalised the observation of a clear expansion in incipient fluidisation conditions, especially when large grain sizes were used. Nevertheless, the effect of the nozzle design on the height of the expanded bed was of limited relevance, indicating that the superficial velocity attained in the main filter body became the main factor for the fluidisation process. Interestingly, the observed bed expansion function as a function of the superficial velocity for silica sand media developed a zone at intermediate v_s values where the slope slowed down. This region was not observed for microspheres.

Related to the fluidisation dynamics, the video recordings exhibited a more uniform behaviour of the expanded bed at low and moderate flow rates when using the new nozzle design, likely due to its high open area. However, at high flow rates ($v_s > 100$ m h^{-1}), the media experienced a more intense turbulent behaviour with the new nozzle than with the commercial one, increasing the measured variability of the fluidised bed height. The new nozzle design reduced the pressure drop in the backwashing regime by 65% (averaged value for all media types and packed bed heights tested) with respect to the commercial nozzle at $v_s \approx 80$ m h^{-1}.

Analytical models of the pressure drop with tap water in filtration mode as well as of the height of the expanded bed in backwashing, as a function of the superficial velocity, were developed. Both expressions reasonably reproduced the observed data, though clearly failing to determine the velocity at the onset of the fluidisation process. However, both models revealed as positive tools to infer the behaviour of the pressurised porous media filter analysed. Nevertheless, additional studies are needed to propose the use of these models for commercial units, such as ones with filters with larger cross-sectional areas.

Supplementary Information The online version contains supplementary material available at https://doi.org/10.1007/s00271-024-00985-9.

Acknowledgements J. Graciano-Uribe acknowledges the support of the IFUdG342022 fund. Open Access funding provided thanks to the CRUE-CSIC agreement with Springer. Jordi Vicens and Sergi Saus provided very helpful technical assistance.

Author contribution J.G. and M.D. conducted the experimental tests. J.G., and F.R.C. carried out the data processing. J.G. and T.P. wrote the main manuscript text. J.G., T.P., G. A., and J.P. developed the analytical models. All authors analysed and discussed the results, and reviewed the manusctript.

Funding Open Access funding provided thanks to the CRUE-CSIC agreement with Springer Nature.

Data availability Data are available on request from the corresponding authors.

Declarations

Conflict of interest The authors declare no conflict of interest.

References

Alcon GD, de Deus FP, Diotto AV, Thebaldi MS, Mesquita M, Nana Y, Baptistella Zueleta NA (2023) Influence of the diffuser plate construction design on the filtration hydraulic behaviour in a pressurized sand filter. Biosys Eng 233:114–124. https://doi.org/10.1016/j.biosystemseng.2023.07.012

Amirtharajah A (1971) Optimum expansion of sand filters during backwash. In: PhD dissertation, Iowa State University, Ames, USA

Anyango GW, Bhowmick GD, Bhattacharya NS (2024) A critical review of irrigation water quality index and water quality management practices in micro-irrigation for efficient policy making. Desalin Water Treat 318:100304. https://doi.org/10.1016/j.dwt.2024.100304

Bové J, Arbat G, Duran-Ros M, Pujol T, Velayos J, Ramírez de Cartagena F, Puig-Bargués J (2015) Pressure drop across sand and recycled glass media used in micro irrigation filters. Biosys Eng 137:55–63. https://doi.org/10.1016/j.biosystemseng.2015.07.009

Brouckaert BM (2004) Hydrodynamic detachment of deposited particles in fluidized bed filter backwashing. In: PhD dissertation, Georgia Institute of Technology, Atlanta, USA

Burt C (2010) Hydraulics of commercial sand media filter tank used for agricultural drip irrigation. ITCR Report No. R 10001. San Luis Obispo, CA, USA: Irrigation Training and Research Center

Cruz-Matías I, Ayala D, Hiller D, Gutsch S, Zacharias M, Estradé S, Peiró F (2019) Sphericity and roundness computation for particles using the extreme vertices model. J Comput Sci. https://doi.org/10.1016/j.jocs.2018.11.005

de Deus FP, Testezlaf R, Mesquita M (2016) Assessment methodology of backwash in pressurized sand filters. Revista Brasileira De Engenharia Agrícola e Ambiental 20(7):600–605. https://doi.org/10.1590/1807-1929/agriambi.v20n7p600-605

de Deus FP, Mesquita M, Salcedo Ramirez JC, Testezlaf R, de Almeida RC (2020) Hydraulic characterisation of the backwash process in sand filters used in micro irrigation. Biosys Eng 192:188–198. https://doi.org/10.1016/j.biosystemseng.2020.01.019

Duran-Ros M, Pujol J, Pujol T, Cufí S, Arbat G, Ramírez de Cartagena F, Puig-Bargués J (2023) Solid removal across the bed depth in media filters for drip irrigation systems. Agriculture 13(2):458. https://doi.org/10.3390/agriculture13020458

Erdim E, Akgiray Ö, Demir I (2015) A revisit of pressure drop-flow rate correlations for packed beds of spheres. Powder Technol 283:488–504. https://doi.org/10.1016/j.powtec.2015.06.017

Graciano-Uribe J, Pujol T, Puig-Bargués J, Duran-Ros M, Arbat G, Ramírez de Cartagena F (2021) Assessment of different pressure drop-flow rate equations in a pressurized porous media filter for irrigation systems. Water 13:2170. https://doi.org/10.3390/w13162179

Graciano-Uribe J, Pujol T, Hincapie-Zuluaga D, Puig-Bargués J, Duran-Ros M, Arbat G, Ramírez de Cartagena F (2022) Bed expansion at backwashing in pressurised porous media filters for drip irrigation: numerical simulations and analytical equations. Biosys Eng 223:277–294. https://doi.org/10.1016/j.biosystemseng.2022.09.008

Graciano-Uribe J, Pujol T, Duran-Ros M, Arbat G, Ramírez de Cartagena F, Puig-Bargués J (2024) Effects of porous media type and nozzle design on the backwashing regime of pressurised porous media filters. Biosys Eng 247:77–90. https://doi.org/10.1016/j.biosystemseng.2024.09.005

Herzig JP, Leclerc DM, Le Goff P (1970) Flow of suspensions through porous media. Ind Eng Chem 62(5):8–35. https://doi.org/10.1021/ie50725a003

Holzer L, Marmet P, Fingerle M, Wiegmann A, Neumann M, Schmidt V (2023) Tortuosity and microstructure effects in porous media. Classical theories, empirical data and modern methods. Springer, Cham, p 333. https://doi.org/10.1007/978-3-031-30477-4

Hunce SY, Soyer E, Akgiray Ö (2019) Use of filterability index in granular filtration: effect of filter medium type, size and shape. Water Supply 19:382–391. https://doi.org/10.2166/ws.2018.083

Ives KJ (1970) Rapid filtration. Water Res 4:201–223. https://doi.org/10.1016/0043-1354(70)90068-0

Kramer OJI, de Moel PJ, Baars ET, van Vugt WH, Padding JT, van der Hoek JP (2019) Improvement of the Richardson-Zaki liquid-solid fluidization model on the basis of hydraulics. Powder Technol 343:465–478. https://doi.org/10.1016/j.powtec.2018.11.018

Kramer OJI, de Moel PJ, Padding JT, Baars ET, El Hasadi YMF, Boek ES, van der Hoek JP (2020a) Accurate voidage prediction in fluidisation systems for full-scale drinking water pellet softening reactors using data driven models. J Water Proc Eng 37:101481. https://doi.org/10.1016/j.jwpe.2020.101481

Kramer OJI, Padding JT, van Vugt WH, de Moel PJ, Baars ET, Boek ES, van der Hoek JP (2020b) Improvement of voidage prediction in liquid-solid fluidized beds by inclusion of the froude number in effective drag relations. Int J Multiph Flow 127:103261. https://doi.org/10.1016/j.ijmultiphaseflow.2020.103261

Lamm FR, Ayars JE, Nakayama FS (2007) Microirrigation for crop production. Design Operation, and Management. Elsevier, Amsterdam

McCabe WL, Smith JC, Harriot P (1993) Unit operations in chemical engineering, 5th edn. McGraw-Hill, Inc., New York

Meniconi S, Brunone B, Mazzetti E, Laucelli DB, Borta G (2016) Pressure reducing valve characterization for pipe system management. Procedia Eng 162:455–462. https://doi.org/10.1016/j.proeng.2016.11.088

Mesquita M, Testezlaf R, Ramirez JCS (2012) The effect of media bed characteristics and internal auxiliary elements on sand filter head loss. Agric Water Manag 115:178–185. https://doi.org/10.1016/j.agwat.2012.09.003

Mesquita M, Testezlaf R, de Deus FP, da Rosa LM (2017) Characterization of flow lines generated by pressurized sand filter underdrains. Chem Eng Trans 58:715–720. https://doi.org/10.3303/CET1758120

Mesquita M, de Deus FP, Testezlaf R, Diotto AV (2019a) Removal efficiency of pressurized sand filter during the filtration process. Desalin Water Treat 161:132–143. https://doi.org/10.5004/dwt.2019.24285

Mesquita M, de Deus FP, Testezlaf R, da Rosa LM, Diotto AV (2019b) Design and hydrodynamic performance testing of a new pressure sand filter diffuser plate using numerical simulation. Biosys Eng 183:58–69. https://doi.org/10.1016/j.biosystemseng.2019.04.015

Moffat RJ (1988) Describing the uncertainties in experimental results. Exp Thermal Fluid Sci 1:2–17. https://doi.org/10.1016/0894-1777(88)90043-X

Pujol T, Arbat G, Bové J, Puig-Bargués J, Duran-Ros M, Velayos J, Ramírez de Cartagena F (2016) Effects of the underdrain design on the pressure drop in sand filters. Biosys Eng 150:1–9. https://doi.org/10.1016/j.biosystemseng.2016.07.005

Pujol T, Puig-Bargués J, Arbat G, Duran-Ros M, Solé-Torres C, Pujol J, Ramírez de Cartagena F (2020a) Effect of wand-type underdrains on the hydraulic performance of pressurised sand media filters. Biosys Eng 192:176–187. https://doi.org/10.1016/j.biosystemseng.2020.01.015

Pujol T, Puig-Bargués J, Arbat G, Vegas A, Duran-Ros M, Pujol J, Ramírez de Cartagena F (2020b) Numerical study of the effects of pod, wand and spike type underdrain systems in pressurised sand filters. Biosys Eng 200:338–352. https://doi.org/10.1016/j.biosystemseng.2020.10.018

Pujol T, Duran-Ros M, Arbat G, Cufí S, Pujol J, Ramírez de Cartagena F, Puig-Bargués J (2024) Pressurised sand bed filtration model: set up and energy requirements for a filtration cycle. Biosys Eng 238:62–77. https://doi.org/10.1016/j.biosystemseng.2024.01.001

Richardson JF, Zaki WN (1954) Sedimentation and fluidization, part I. Transactions of the Institute of Chemical Engineering 32:35–53

Solé-Torres C, Puig-Bargués J, Duran-Ros J, Arbat G, Pujol J, Ramírez de Cartagena F (2019) Effect of underdrain design, media height and filtration velocity on the performance of microirrigation sand filters using reclaimed effluents. Biosys Eng 187:292–304. https://doi.org/10.1016/j.biosystemseng.2019.09.012

Song L, Cai J, Zhai G, Feng J, Fan Y, Han J, Hao P, Ma N, Miao F (2024) Comparative study and evaluation of sediment deposition and migration characteristics of new sustainable filter media in micro-irrigation sand filters. Sustainability 16:3256. https://doi.org/10.3390/su16083256

Tao H, Wu Z, Zhou Y, Li Q, Aihemaiti M, Jiang Y, Yang W (2023) Establishment of a dimensional analysis-based prediction model for the head loss of pre-pump micro-pressure filters for micro-irrigation. Irrig Sci 41:803–815. https://doi.org/10.1007/s00271-023-00879-2

White FM (2009) Fluid Mechanics, 7th edn. McGraw-Hill, Inc., New York

Yazdchi K, Luding S (2012) Towards unified drag laws for inertial flow through fibrous materials. Chem Eng J. https://doi.org/10.1016/j.cej.2012.06.140

Zamani A, Maini B (2009) Flow of dispersed particles through porous media—deep bed filtration. J Petrol Sci Eng 69:71–88. https://doi.org/10.1016/j.petrol.2009.06.016

Zhang W, Cai J, Zhai G, Song L, Lv M (2023) Experimental study on the filtration characteristics and sediment distribution influencing factors of sand media filters. Water 15:4303. https://doi.org/10.3390/w15244303